Phase field study of interfacial diffusion-driven spheroidization in a composite comprised of two mutually insoluble phases

Liang Tian[1,2,a)] and Alan Russell[1,2]
[1]*Department of Materials Science and Engineering, Iowa State University, Ames, Iowa 50011, USA*
[2]*Ames Laboratory, U.S. Department of Energy, Ames, Iowa 50011, USA*

(Received 31 January 2014; accepted 12 March 2014; published online 27 March 2014)

The phase field approach is a powerful computational technique to simulate morphological and microstructural evolution at the mesoscale. Spheroidization is a frequently observed morphological change of mesoscale heterogeneous structures during annealing. In this study, we used the diffuse interface phase field method to investigate the interfacial diffusion-driven spheroidization of cylindrical rod structures in a composite comprised of two mutually insoluble phases in a two-dimensional case. Perturbation of rod radius along a cylinder's axis has long been known to cause the necessary chemical potential gradient that drives spheroidization of the rod by Lord Rayleigh's instability theory. This theory indicates that a radius perturbation wavelength larger than the initial rod circumference would lead to cylindrical spheroidization. We investigated the effect of perturbation wavelength, interfacial energy, volume diffusion, phase composition, and interfacial percentage on the kinetics of spheroidization. The results match well with both the Rayleigh's instability criterion and experimental observations. © *2014 AIP Publishing LLC*. [http://dx.doi.org/10.1063/1.4869296]

I. INTRODUCTION

Many two-phase composites consist of a cylindrical rod phase embedded inside a matrix phase.[1–3] These cylindrical rods tend to break up into spheres during annealing treatment.[1,3,4] Such spheroidization has a large effect on material properties.[4–8] For example, spheroidization of the filamentary phase in deformation processed metal-metal composites (e.g., Al-20%Sn composite[5]) lowers the strength and electrical conductivity[7] of the composite. The isothermal magnetization curve of Cu-Nb *in situ* composites also depends on the spheroidization kinetics.[7] For metallic nanowires used in microelectronics, fragmentation of the nanowires into chains of nanospheres would affect its electrical, chemical, and thermal properties.[4] In Al-Si alloys, the spheroidization of eutectic silicon resulted in outstanding fracture strain with good yield strength.[6] Thus, the stability of various properties of these materials depends on their morphological stability.

The first investigation of the break-up of rods into spheres was done by Lord Rayleigh when he studied the instability of jets of fluids.[8] Lord Rayleigh introduced a tiny longitudinal perturbation of rod radius in a single harmonic form: $r = R + \delta\cos(\frac{2\pi x}{\lambda})$, where R is the initial unperturbed rod radius, δ is the amplitude of the perturbation, λ is the perturbation wavelength, and x is the distance along the rod axis. δ was assumed to be small to validate the small-surface-slope approximation.[9] Lord Rayleigh[8] predicted that a cylinder with radius R would be unstable against the perturbation and would spheroidize when the perturbation wavelength λ is larger than the initial rod circumference $2\pi R$ due to the minimization of surface free energy. The perturbation wavelength with the fastest spheroidization rate, λ_m, was predicted to be 9.016 R. If the initial perturbation is multi-harmonic, this fastest-growing perturbation will dominate and determine the final average spacing and sphere size.[9]

In Rayleigh's theory, only surface diffusion is considered to drive the spheroidization due to volume conservation constraint so that surface free energy is the total free energy to be minimized. If the specific surface energy is independent of crystallographic orientation, the minimization of surface free energy is equivalent to the minimization of surface area of the phase (i.e., forming a spherical surface).[10] This isotropic surface energy density assumption is a good approximation for amorphous and untextured polycrystalline materials. In the case of orientation-dependent specific surface energy (e.g., single-crystal materials), the equilibrium shape due to minimization of surface free energy can be determined by the well-known Wulff construction based on the Gibbs-Wulff theorem by using a polar plot of the surface energy density (gamma plot).[11] From a mechanistic perspective, the driving force of surface diffusion for spheroidization is the chemical potential difference between surface atoms.[5] The chemical potential of an atom on a curved surface can be derived from the Gibbs-Thompson equation, $\mu = \mu_0 + \gamma V\kappa$, where μ_0 is the chemical potential of an atom on a flat surface, γ is the surface energy density, V is the atomic volume, and κ is the surface curvature.[5,11] κ can be calculated by the direct sum of two principal curvatures κ_1 and κ_2. κ_1 is determined by perturbated rod radius and κ_2 is determined by the perturbation wavelength and amplitude. The total curvature determining the chemical potential is a competition between κ_1 and κ_2, which can be mathematically simplified to be a competition between the unperturbated rod radius and the perturbation itself.[5] The competition between unperturbated radius

a)Author to whom correspondence should be addressed. Electronic mail: ltian@iastate.edu. Tel.: +1-515-509-0857. Present address: 2220 Hoover Hall, Iowa State University, Ames, Iowa 50011, USA.

and the perturbation itself can lead to the Rayleigh instability criterion. It clearly explains why radius perturbation is necessary to generate the chemical potential gradient for the cylinder to spheroidize by surface diffusion. A similar explanation of this competition can be understood by the Young-Laplace equation utilizing the pressure-driving mechanism. Another way to understand the Rayleigh instability is that a critical intermediate perturbation stage exists so that before this stage, the growing of perturbation would increase the surface area of the system and would therefore be energetically unfavorable. After this stage, further growth of the perturbation would decrease the surface area substantially and lead to break-up of spheres even though spheres are initially more energetically favorable than rods.[2]

The atomistic mechanism of spheroidization for the discussion above is a surface diffusion mediated kinetic process.[12] According to Ref. 10, the available mechanisms for morphological change include surface diffusion, volume diffusion (e.g., Ostwald ripening), evaporation, and condensation. Nichols and Mullins investigated the contributions of both surface/interface and volume diffusion to the morphological changes and found that the surface diffusion is the dominating mechanism for shape change.[13] The influence of volume diffusion on morphological changes has attracted considerable attention recently.[14–16] It is our motivation in this paper to study the combined effect of both surface/interface diffusion and volume/bulk diffusion (i.e., compositional change driven by minimization of interfacial and bulk free energy, respectively) on the spheroidization of two insoluble phase systems. The diffuse interface phase field model is used to study diffusion-controlled phase morphology evolution by using a conserved compositional phase field variable. The temporal and spatial evolution of the compositional field is governed by the Cahn-Hilliard nonlinear partial differential equation. The interface diffusion mechanism is explicitly implemented in the free energy functional as interfacial free energy. By setting the initial interface microstructure, the interface related and bulk related chemical potential can be determined with time evolution to estimate the role of interface diffusion and volume diffusion to the kinetic spheroidization process. Though initially the interface diffusion is the only operating mechanism in our model, bulk diffusion (i.e., phase separation in insoluble systems) begins to play a role as time progresses. Our goal is to evaluate the effect of volume diffusion on spheroidization kinetics in these systems. The Rayleigh instability criterion for spheroidization will then be compared with our simulation results to verify its applicability in diffusion-controlled morphology change. The effect of phase composition, interface percentage, and interface energy on the spheroidization kinetics was also investigated.

II. DIFFUSE INTERFACE PHASE FIELD MODEL

The phase field model is a powerful tool to study microstructural evolution at the mesoscale by using a set of conserved and non-conserved continuous phase field variables.[17,18] The diffuse interface description of the phase field model uses the gradients of phase field variables to describe the interface, which allows one to avoid tracking the interface positions as moving boundary conditions and to predict the evolution of arbitrary morphologies and complex microstructures.[17,18] In a sharp interface description, different microstructures are expressed as discrete regions separated by a zero-thickness interface.[19] Zhu *et al.* found a good agreement of the kinetics of microstructural evolution between the diffuse interface and shape interface descriptions.[19] The thermodynamic driving force for the field variables includes bulk and interface free energy, elastic, electrostatic, and magnetic energy.[17] The temporal and spatial evolution of phase field variables is described by the Allen-Cahn equation (time dependent Ginzburg-Landau equation) for non-conserved field variables and the nonlinear Cahn-Hilliard equation for conserved field variables.[20] The phase field model can at least qualitatively explain the experimental observations in the absence of a complete set of real thermodynamic and kinetic parameters, which can be difficult to obtain from experiments or more expensive atomistic simulations.[19] This approach has been widely used in modeling grain growth, spinodal decomposition, solidification, solid state phase transformations, etc.[20]

The system in this study is the simplest isostructural two-phase system that needs only a single compositional field to describe the microstructure.[21,22] In this system, the free energy dependence on structure-related field variables (grain boundaries, dislocations, etc.) is neglected because the driving force for the spheroidization is atomic diffusion. For untextured polycrystalline materials, these structure-related field variables would change only the kinetic parameters for atomic diffusion, which can be described well by atomic mobility, temperature, and the interfacial energy coefficient in our model. So, the effects of these complex structural characteristics can be incorporated qualitatively in the above kinetic parameters. Isotropic interfacial energy coefficient and mobility will be assumed in our model to simplify the calculation. The effect of grain boundaries (i.e., grain growth) in two polycrystalline phase systems on the diffusion kinetics could be investigated in the future in both isotropic and anisotropic grain boundary energy cases.

In the diffuse interface phase field model, interfacial energy is incorporated by the gradients of phase field variables, so the total free energy, F, of our inhomogeneous system is given by[23]

$$F = \int_V \left[f(c, T) + \frac{1}{2}\alpha (\nabla c)^2 \right] dV \tag{1}$$

where $f(c, T)$ is the local free energy density, $\frac{1}{2}\alpha (\nabla c)^2$ is the interfacial free energy density, c is the compositional field, T is the temperature of the system, and α is the interfacial energy coefficient which substantially affects the kinetics of compositional evolution. We assume α to be an isotropic constant. The local free energy density function of a two-phase binary system can be determined from real thermodynamic data. But since we are interested only in modeling the morphological evolution, a simple double well potential[21–23] can be used as

$$f(c, T) = \left(\frac{1}{4}c^4 - \frac{1}{2}c^2 \right) \frac{T}{\tau}, \tag{2}$$

where τ is a phenomenological parameter introduced as a reference temperature, which characterizes the entropy of the system according to thermodynamics.[24] The local free energy density has two degenerate minima at 1 representing phase A and at -1 representing phase B. By adopting this form of local free energy density, the local free energy minimization tends to de-mix two phases, and the two-phase system has no mutual solubility. In this study, temperature is an input parameter that affects the kinetics of the system, chosen to be $T = \tau$ when the temperature effect was not studied. Under this temperature setting, the potential well depth is $\frac{1}{4}$ in Eq. (2). The potential well depth is allowed to be changed independently of temperature in this study by adding a proportional constant in Eq. (2). It would also determine the relative role of bulk diffusion to the compositional evolution.

The local chemical potential of each molecule can be given by[20,21]

$$\mu = \frac{1}{N_V}\frac{\delta F}{\delta c} = \frac{1}{N_V}\left(\frac{\partial f}{\partial c} - \alpha\nabla^2 c\right), \tag{3}$$

where N_V is the number density (number of molecules per unit volume) and $\frac{\delta F}{\delta c}$ is the functional derivative. The chemical potential is contributed by two parts: the first part, $\frac{1}{N_V}\frac{\partial f}{\partial c}$, depends only on local composition, which would be responsible for driving bulk diffusion; the second part, $\frac{\alpha}{N_V}\nabla^2 c$, depends on both the local and neighboring composition fields, which drive interfacial diffusion. Under the small slope approximation (i.e., gradual compositional change across a diffuse interface), the second derivative of compositional field in space can be used to characterize the curvature of the interface. Therefore, the second part of the chemical potential, $\frac{\alpha}{N_V}\nabla^2 c$, is similar to the chemical potential on a curved surface, $\gamma V\kappa$, by the Gibbs-Thompson equation, where α and γ stand for interfacial energy and $\frac{1}{N_V} = V$. The total chemical potential is a competition between interface and bulk-related chemical potential contribution. Our goal, therefore, is to investigate the dominating chemical potential gradient, contributed by either the bulk- or interface-related potential term, when spheroidization occurs.

The kinetics of diffusion can be described by Fick's First Law, which relates the diffusion flux J to the chemical potential gradient as

$$J = -N_V M\nabla\mu, \tag{4}$$

where M is the atomic mobility, assumed to be constant. The mass conservation constraint for conserved field variables requires

$$\frac{\partial c}{\partial t} = -\nabla J. \tag{5}$$

Therefore, the temporal and spatial evolution equation of the compositional field variable can be derived by combining Eqs. (2) and (5) as

$$\frac{\partial c}{\partial t} = M\nabla^2\left(\frac{\partial f}{\partial c} - \alpha\nabla^2 c\right) = M\nabla^2\left[(c^3 - c)\frac{T}{\tau} - \alpha\nabla^2 c\right]. \tag{6}$$

Equation (6) is called the Cahn-Hilliard equation. By numerically solving this nonlinear partial differential equation, we can describe the diffusion-controlled morphological evolution of an isostructural, two-phase system. Like most phase field simulations, we employ the second order finite difference discretization in space and explicit forward Euler method for time.[23] The temperature, interfacial energy coefficient, and mobility in this equation are just parameters affecting the diffusion kinetics.

III. NUMERICAL SIMULATION RESULTS

The numerical simulations are done in a two-dimensional (2D) square lattice with grid size $a = 1$. The finite difference algorithm to evaluate the Laplacian in 2D is given by[20]

$$\nabla^2 c(i,j) = \frac{1}{2a^2}\left[\sum\nolimits_{NN} c(i,j) + \frac{1}{2}\sum\nolimits_{NNN} c(i,j) - 6 * c(i,j)\right], \tag{7}$$

where i,j indicates the position of the interested grid point, NN stands for the nearest neighbor, and NNN stands for the next nearest neighbor. The time evolution of composition is given by the forward Euler method as

$$c(i,j,t+dt) = c(i,j,t) + \frac{\partial c}{\partial t}(i,j,t) * dt. \tag{8}$$

The initial microstructures are set up as alternating complete phase A and phase B regions separated by single harmonic interfaces. Under this setting, the initial interfacial diffusion that drives mixing would be opposed against by the subsequent bulk diffusion that drives de-mixing. The cylindrical rod phase A would become rectangular in the longitudinal cross section for a 2D simulation. So, if the perturbated rod radius of phase A is $R_A + \delta\sin(2\pi\frac{x}{\lambda})$, then the perturbated rod radius of phase B would be $R_B - \delta\sin(2\pi\frac{x}{\lambda})$. The effect of phase composition $\frac{R_A}{R_B}$ and perturbation wavelength λ on shape change will be investigated in the following context. All simulations use periodic boundary conditions for all boundaries to eliminate the system-size effect.

A. The effect of perturbation wavelength-applicability of Rayleigh instability criterion

The Rayleigh instability criterion claims that a rod would spheroidize if the perturbation wavelength λ is larger than the circumference of the unperturbated rod; otherwise it would smooth down. In a 2D case, the circumference of the unperturbated rod would be $2R_A$. In order to investigate if the combined diffusion-controlled morphology change satisfies this criterion, the following parameters are set up for the simulation: $M = 1$, $T^* = \frac{T}{\tau} = 1$, and $\alpha = 15$. It is worthwhile to mention that in this study, we are only interested in qualitatively simulating the spheroidization phenomenon in two phase composites so that accurate input of all model parameters is not our concern. Therefore, the units of all input parameters and physical variables are neglected to avoid the wrong impression that the simulation is done quantitatively for a real physical system with input parameters coming from

real thermodynamic and kinetic dataset. The system size is 100 by 100. Unperturbated rod radius $R_A = R_B = 10$, which suggests that the volume fraction of phase A is 50%, and the interfacial grid points account for 20% of the total grid points. The time step should be chosen small enough to maintain convergence and accuracy, large enough to reduce computational load and simulate long time duration. Here dt is chosen as 4×10^{-3}. The perturbation amplitude $\delta = 2$. Three different perturbation wavelengths $\lambda = 12.5, 20, 25$ are chosen to evaluate its effect on compositional evolution to determine if the Rayleigh instability criterion is applicable in this diffusion-controlled process.

The simulation results are given in Fig. 1. When the perturbation wavelength $\lambda = 12.5$ (see Fig. 1(a)) is less than the circumference $2R_A$ of 2D unperturbated rod, the compositional profile flattens out. When $\lambda = 20$ is equal to $2R_A$, the compositional field begins to show some tendency toward spheroidization. When $\lambda = 25$ is larger than $2R_A$, the compositional field becomes spheroidized. The simulation results show an obvious transition of compositional field from flattening to spheroidizing after a perturbation wavelength sweep from smaller than $2R_A$ to larger than $2R_A$, which matches the description of Rayleigh instability criterion. From Fig. 1, it can also be concluded that the compositional field of a strongly curved interface (smaller λ in Fig. 1(a)) tends to become evenly distributed more quickly than that for a larger λ in Figs. 1(b) and 1(c). This can be explained by the fact that strongly curved interface has a larger initial chemical potential gradient, which acts as a larger driving force for diffusion to occur more rapidly. The experimental evidence of the applicability of Rayleigh instability criterion in spheroidization of two phase composites can be found in Refs. 25 and 26 which clearly showed that the spheroidized Nb rod had perturbation wavelength larger than the initial rod circumference.

The next thing to confirm is whether the interface-related chemical potential gradient in Eq. (3) is the major driving force for the shape-change process. Therefore, the interface-related and bulk-related chemical potential distributions in the case of Fig. 1(c) at 1000 and 3000 time steps are given in Fig. 2. The interface-related chemical potential gradient is roughly 2.8 and 2 times of its bulk-related counterpart at 1000 and 3000 time steps, respectively. Similar results can be obtained in the case of Fig. 1(a), but have not been included to reduce redundancy. This suggests that the interface-related chemical potential gradient is the major driving force for the shape-reforming process, and it decreases more rapidly than the bulk-related chemical potential gradient as time progresses. This conclusion seems to match the previous statement in Refs. 12, 13, and 16 that the surface/interface diffusion is the dominating mechanism for the morphological change.

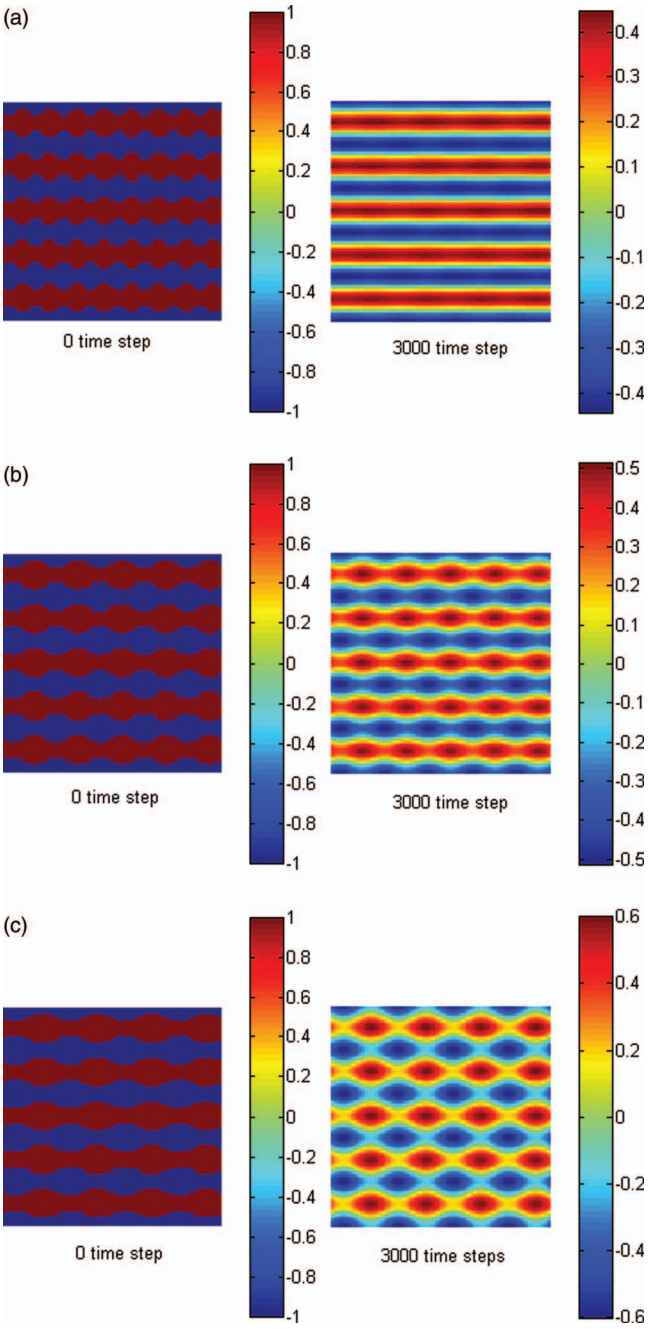

FIG. 1. The composition evolution in a two-phase system with size 100 by 100. The volume fraction of phase A (red) is 50%. The interface between phase A and phase B (blue) is a single harmonic perturbation with perturbation amplitude $\delta = 2$. Unperturbated rod radius $R_A = R_B = 10$. Time step $dt = 4 \times 10^{-3}$. (a) Perturbation wavelength $\lambda = 12.5$, (b) perturbation wavelength $\lambda = 20$, and (c) perturbation wavelength $\lambda = 25$.

B. The effect of interfacial energy coefficient

In Sec. III A, the interfacial energy coefficient, α, is large so that compositional evolution is driven by a large interfacial chemical potential gradient to minimize the free energy as interpreted from Eq. (6). The kinetics of the composition evolution should be directly affected by the value of α. Therefore, three different α values are chosen to compare with the result in Fig 1(c) to investigate the effect of α on spheroidization kinetics. The parameters are set up the same as in Fig. 1(c) except for the interfacial energy coefficient. The results of the compositional fields at 3000 time steps are given in Fig. 3, which clearly shows that a larger interfacial energy coefficient will yield a larger interfacial chemical potential (see

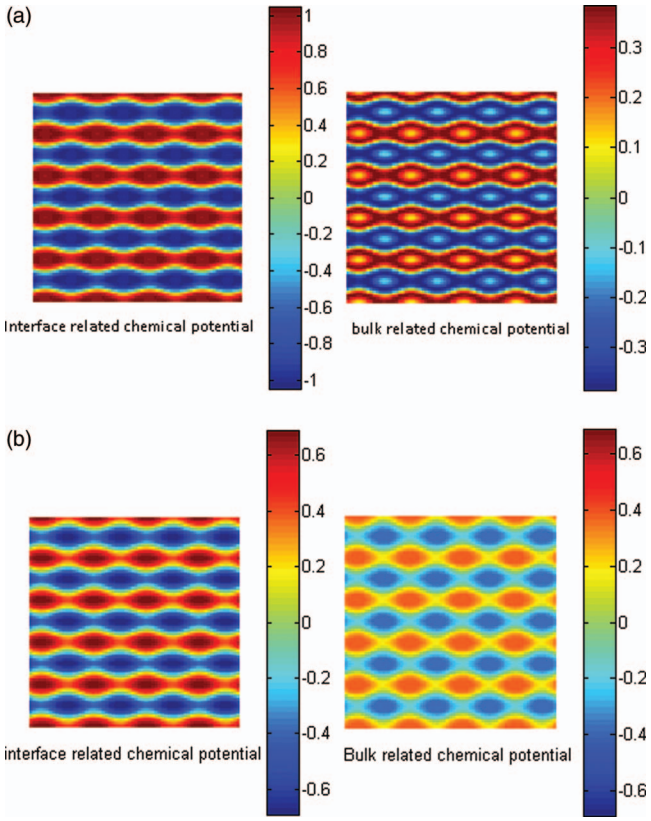

FIG. 2. The interface-related and bulk-related chemical potential distributions in the case of Fig. 1(c) at 1000 time steps (a) and 3000 time steps (b), respectively.

Eq. (6)) to drive the spheroidization of the compositional field faster.

C. The effect of volume diffusion

From Sec. III A, interfacial chemical potential is the major driving force for spheroidization. But the effect of volume diffusion on spheroidization is still unclear. In order to investigate the volume diffusion effect, we chose three double-well potentials with different potential well depths 0, 0.5, and 1 to compare with the result in Fig. 1(c) with potential well depth $\frac{1}{4}$. The other parameters are the same as those in Fig. 1(c). The results from these three potential well depths at 3000 time steps are given in Fig. 4. Combining Figs. 4 and 1(c), it can be easily seen that as well depths increased from 0 to 1, the role of bulk free energy increased according to Eq. (2); therefore, the bulk-related chemical potential will increase and become comparable with the interface-related chemical potential. The bulk chemical potential tends toward de-mixing the two phases, which suppresses the compositional mixing driven by interfacial diffusion that favors a spheroidized compositional field. As a result, the spheroidization kinetics slows down substantially due to the less dominating role of interfacial diffusion. This is consistent with the previous conclusion that interface diffusion is the dominating mechanism for morphological change. For the case where well-depth is 0 (i.e., no volume diffusion, see Fig. 4(a)), the compositional spheroidization is much faster than that with a finite well-depth potential including the volume-diffusion effect. To summarize, the role of volume diffusion is to compete with interface diffusion to slow the spheroidization kinetics. If interfacial diffusion is dominating, the spheroidization occurs rapidly; otherwise, spheroidization will slow down substantially.

The effect of temperature on the spheroidization kinetics can be understood in a similar way as the effect of potential well depth when considering volume diffusion. According to Eq. (2), increasing temperature would essentially have the same effect on increasing volume diffusion as increasing potential well depth by a linear temperature dependence of bulk free energy under a constant-entropy approximation. On the contrary, previous studies[27,28] showed that increasing temperature would decrease the interfacial energy. The combined effect of these two would be unfavorable to spheroidization. It has been experimentally observed that coarsening is more favored than spheroidization at high temperature in Cu-Nb system.[7] Raabe and Ge[29] also observed that the initially heavily curled Cr filaments in Cu-Ag matrix undergo a morphological transition from spheroidization to competitive coarsening at 1273 K for 4 h. Since the temperature dependence of the interfacial energy is much more diverse and system-dependent,[27,28] there is some complexity and uncertainty when evaluating the temperature effect.

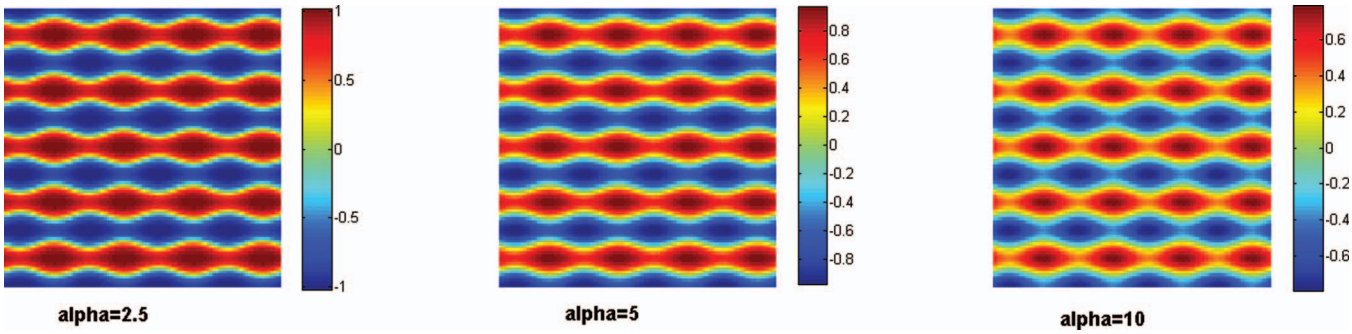

FIG. 3. The compositional field profiles at 3000 time steps for three different interfacial energy coefficients: $\alpha = 2.5$ (left), $\alpha = 5$ (middle), and $\alpha = 10$ (right). The other parameters are the same as in Fig. 1(c). By comparing the composition evolution in Figs. 3 and 1(c), it can be concluded that a larger interfacial energy coefficient yields faster spheroidization.

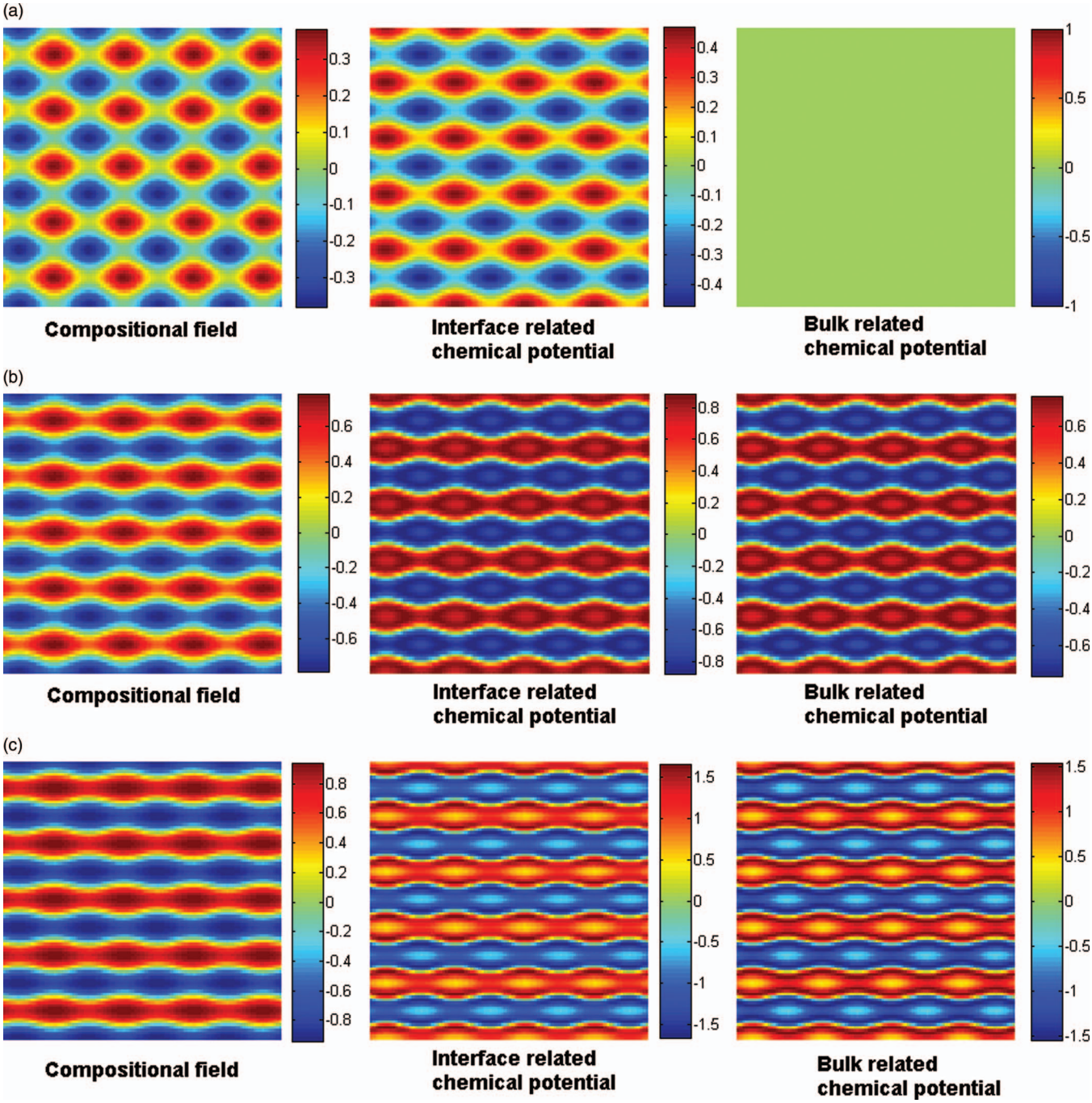

FIG. 4. The compositional field, interfacial chemical potential, and bulk chemical potential at 3000 time steps for three different potential well depths: (a) well depth = 0, (b) well depth = 0.5, and (c) well depth = 1. The other parameters are the same as those in Fig. 1(c) where well depth was 0.25.

D. The effect of phase composition

In previous discussions, the volume fraction of phase A was 50%. In order to investigate the effect of phase composition on the compositional spheroidization, two volume fractions of phase A, 40% and 30%, were chosen. The other parameters for calculation were the same as those in Fig. 1(c). The results of compositional field, interface-related, and bulk-related chemical potentials at 3000 time steps are shown in Fig. 5. By comparing Figs. 1(c), 5(a), and 5(b), it can be concluded that as the volume fraction of phase A decreases, the compositional spheroidization of phase A accelerates. The possible reason is that in all three cases, we have the same amount of interfacial grids (20% of the total), which yields the same initial interfacial diffusion driving forces. The less amount of phase A in Fig. 5(b) would subject its compositional field more to the interfacial diffusion. Therefore, interfacial diffusion plays a more dominating role on phase A in Fig. 5(b) than in Figs. 1(c) and 5(a). This can be directly verified by the relative ratio of interface-related chemical potential to bulk-related chemical potential in Fig. 5. The ratio of interface-related to bulk-related chemical potential of

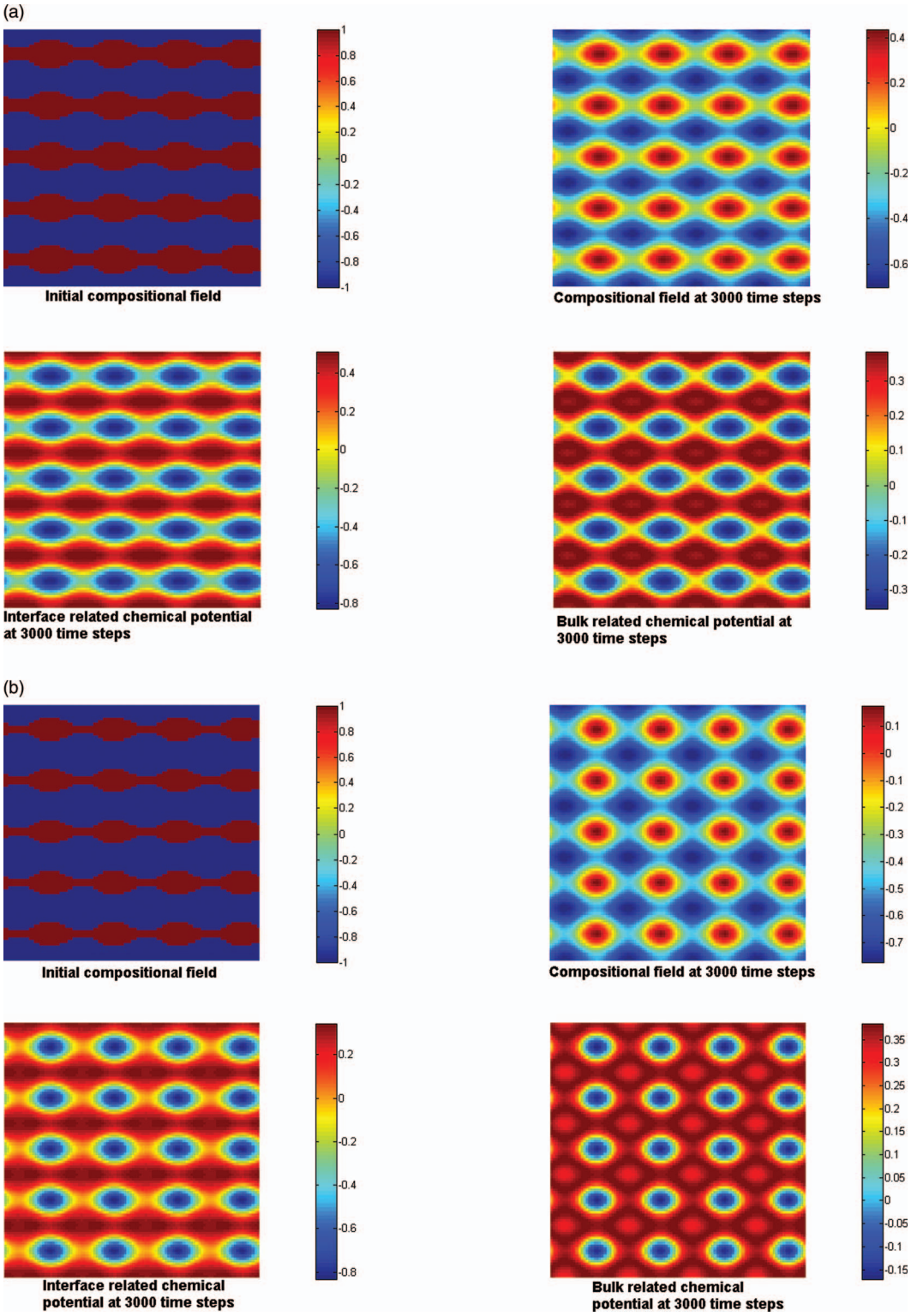

FIG. 5. Two initial compositional fields with different volume fractions of phase A are given to study the effect of phase composition on spheroidization. The other parameters are the same as those in Fig. 1(c). The compositional field, interface-related, and bulk-related chemical potential distributions at 3000 time steps are given: (a) 40 vol.% of phase A and (b) 30 vol.% of phase A.

phase A region in Fig. 5(b) is roughly twice as much as that in Fig. 5(a). As a result, the more dominating interfacial diffusion in phase A of Fig. 5(b) would lead to faster compositional spheroidization of phase A as discussed in Secs. III A–III C. This is consistent with the experimental observations that the minor filament phase is the spheroidized phase.[5–7]

E. The effect of interface area

In the previous discussions (e.g., Fig. 1(c)), the lattice points at the interface account for 20% of the total lattice points in the system. Here, the interface area percentage is chosen to be 8% to be compared with the case in Fig. 1(c) to

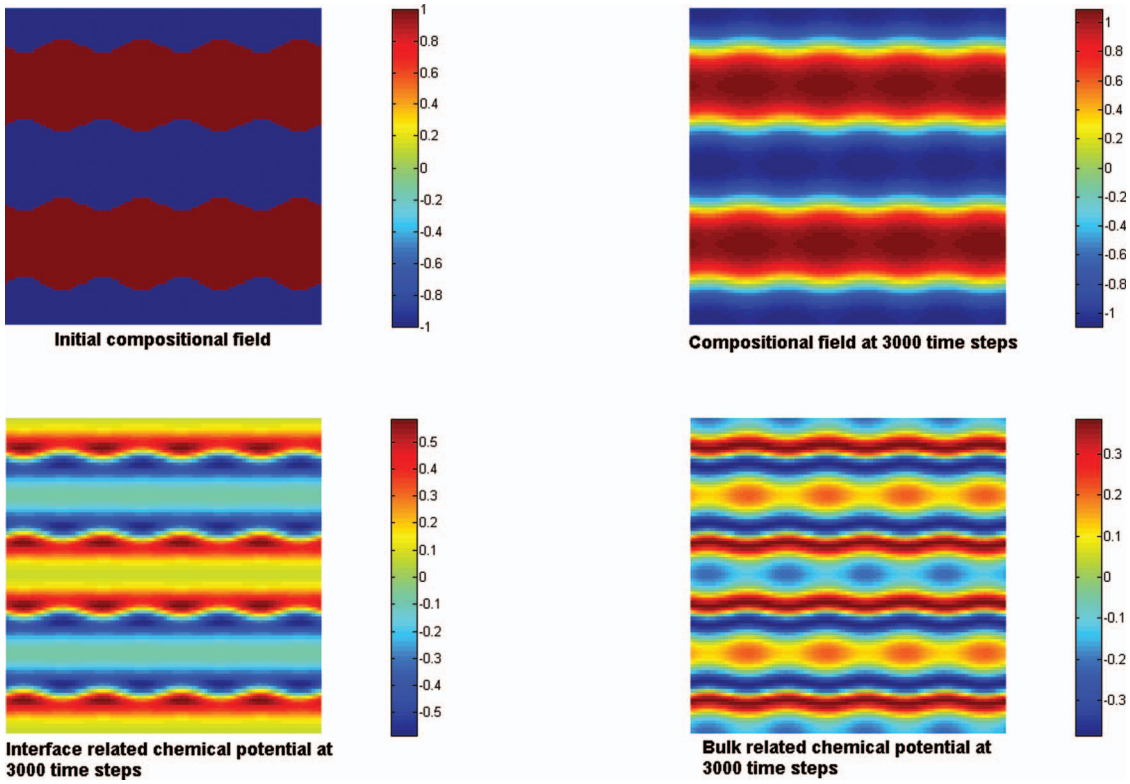

FIG. 6. The compositional field, interface-related, and bulk-related chemical potentials at 3000 time steps for a system with 8% interfacial area. The other parameters are the same as those in Fig. 1(c).

study the effect of interface area on the spheroidization kinetics. All other parameters for calculation are the same as those in Fig. 1(c). The results of compositional field, interface-, and bulk-related chemical potential distributions at 3000 time steps are given in Fig. 6. By comparing Fig. 6 with Fig. 1(c), it can be found that decreasing the interfacial area percentage from 20% to 8% would substantially decrease the spheroidization kinetics. The reason should be that the decreased interfacial area would lower the interfacial diffusion driving force, exerting less effect on the compositional evolution of both phases to be spheroidized. This can be verified by the ratio of interface- to bulk-related chemical potential of phase A in Figs. 2(b) and 6. This ratio in Fig. 6 is 1.5 compared with 2.2 in Fig. 2(b). This decreased interfacial driving force would slow down the compositional spheroidization. Generally, the interfacial area percentage is inversely proportional to the size of filament spacing and/or filament thickness in real systems. The large interfacial area percentage may be the reason why spheroidization is usually experimentally observed in sub-micrometer/nano-size composite systems.[5,7]

IV. CONCLUSIONS

In this paper, the interfacial diffusion-driven spheroidization of a two-phase system containing mutually insoluble phases was studied by the diffuse-interface phase field approach. A single conserved compositional field variable is used to describe the morphological change under an isostructural assumption to simplify calculation. The temporal and spatial evolution of the compositional field is described by the Cahn-Hilliard nonlinear partial differential equations. Under a combined effect of interfacial diffusion and volume diffusion, the system would change its morphology if the interfacial diffusion is the dominating driving force for the compositional evolution. Perturbation of the cylindrical rod radius is a necessity to generate the initial interfacial chemical potential gradient to drive the morphology evolution. Whether the perturbated cylinder will spheroidize or smooth down would depend on the perturbation wavelength and the initial unperturbated rod circumference. According to our simulations, the spheroidization for our system matches very well with the Rayleigh instability criterion. This is a reasonable result since interfacial diffusion is the dominating driving force for morphological evolution in both our study and Rayleigh's theory. Increasing the interfacial energy would enhance the interfacial diffusion contribution and accelerate the spheroidization kinetics. The bulk/volume diffusion driving de-mixing of the two phases seems to impede the spheroidization by competing with the interfacial diffusion. The volume fraction bias between two phases would favor the spheroidization of the minor phase, which has been observed in experiments.[5–7] A size effect also exists for spheroidization kinetics by changing the interfacial area percentage. Spheroidization has been frequently observed in experimental nano-scale composite systems[5,7] because the large interfacial area provides a large driving force for interfacial diffusion.

ACKNOWLEDGMENTS

The financial support of the Iowa State University Research Foundation, the Electric Power Research Center of Iowa State University, and the Department of Energy through

Ames Laboratory Contract No. DE-AC02-07CH11358 is appreciated. The authors are also thankful for the phase field sample code provided by Professor R. Lesar.

[1]H. P. Stuwe and O. Kolednik, Acta Metall. **36**, 1705 (1988).
[2]E. Werner, Acta Metall. **37**, 2047 (1989).
[3]M. Mcleana, Philos. Mag. **27**, 1253 (1973).
[4]M. E. Toimil Molares, A. G. Balogh, T. W. Cornelius, R. Neumann, and C. Trautmann, Appl. Phys. Lett. **85**, 5337 (2004).
[5]X. Kai and A. M. Russell, J. Mater. Sci. **37**, 5209 (2002).
[6]E. Ogris, A. Wahlen, H. Lüchinger, and P. J. Uggowitzer, J. Light Met. **2**, 263 (2002).
[7]M. J. R. Sandim, H. R. Z. Sandim, D. Stamopoulos, R. A. Renzetti, M. G. Das Virgens, and L. Ghivelder, IEEE Trans. Appl. Supercond. **16**, 1692 (2006).
[8]Lord Rayleigh, Proc. London Math. Soc. **10**, 4 (1878).
[9]J. Choy, S. A. Hackney, and J. K. Lee, J. Appl. Phys. **77**, 5647 (1995).
[10]W. Mullins, J. Appl. Phys. **30**, 77 (1959).
[11]C. A. Johnson, Surf. Sci. **3**, 429 (1965).
[12]F. A. Nichols and W. W. Mullins, J. Appl. Phys. **36**, 1826 (1965).
[13]F. A. Nichols and W. W. Mullins, Trans. AIME **233**, 1840 (1965).
[14]E. Ho and G. C. Weatherly, Acta Metall. **23**, 1451 (1975).
[15]T. Courtney and J. Kampe, Acta Metall. **37**, 1747 (1989).
[16]H. L. Duan, *IUTAM Symposium on Scaling in Solid Mechanics* (Springer Netherlands, 2009), Vol. 10, p. 253.
[17]L. Q. Chen, Annu. Rev. Mater. Res. **32**, 113 (2002).
[18]N. Moelans, B. Blanpain, and P. Wollants, CALPHAD: Comput. Coupling Phase Diagrams Thermochem. **32**, 268 (2008).
[19]J. Z. Zhu, T. Wang, S. H. Zhou, Z. K. Liu, and L. Q. Chen, Acta Mater. **52**, 833 (2004).
[20]R. Lesar, *Introduction to Computational Materials Science: Fundamentals to Applications* (Cambridge University Press, NY, 2013).
[21]J. Zhu and L. Q. Chen, Phys. Rev. E **60**, 3564 (1999).
[22]N. Lecoq and H. Zapolsky, Discrete Contin. Dyn. Syst. **2011**, 953 (2011).
[23]D. Raabe, F. Roters, F. Barlat, and L. Q. Chen, *Continuum Scale Simulation of Engineering Materials* (Wiley-VCH, Weinheim, 2004).
[24]D. R. Gaskell, *Introduction to Metallurgical Thermodynamics* (Taylor & Francis, Bristol, PA, 1981).
[25]H. R. Z. Sandim *et al.*, Scr. Mater. **51**, 1099–1104 (2004).
[26]D. Raabe, K. Miyake, and H. Takahara, Mater. Sci. Eng., A **291**, 186–197 (2000).
[27]H. M. Lu and Q. Jiang, J. Phys. Chem. B **109**, 15463 (2005).
[28]J. W. Cahn and J. E. Hilliard, J. Chem. Phys. **28**, 258 (1958).
[29]D. Raabe and J. Ge, Scr. Mater. **51**, 915–920 (2004).